



ISSN 1349-1121  
JAXA-RM-06-015E

JAXA Research and Development Memorandum

---

**Development of Flow Visualization by  
Ultrasonic for Thermocapillary Convection of  
Low Prandtl Number Fluid**

Satoshi MATSUMOTO, Takashi MASHIKO, Hiroaki OHIRA,  
Shinichi YODA, Hiroei SASAKI and Erika YODA

March 2007

Japan Aerospace Exploration Agency



# Development of Flow Visualization by Ultrasonic for Thermocapillary Convection of Low Prandtl Number Fluid

By

Satoshi MATSUMOTO<sup>\*</sup>, Takashi MASHIKO<sup>\*</sup>, Hiroaki OHIRA<sup>\*</sup>,  
Shinichi YODA<sup>\*</sup>, Hiroei SASAKI<sup>\*\*</sup> and Erika YODA<sup>\*\*\*</sup>

**Abstract:** This paper describes an investigation for development of visualization system which aims to observe Marangoni convection in a half-zone liquid bridge of low-Prandtl number fluid of molten tin. Generally, low Prandtl number fluids (eg. molten metal and semiconductor) are opaque. So, the internal flow can not be measured by using a visible light. Therefore we employed the ultrasonic wave to track the particle position. The transducer was made by LiNbO<sub>3</sub> single crystal as a piezoelectric element which was attached on titanium shoe. The suitable tracer to mix into the molten tin liquid bridge was examined in several points of view; density match, wettability with mother fluid, acoustic impedance and so on. The hollow Shirasu-balloon coated with Ni and Fe could be made. The feasibility test of this system was performed and the result demonstrates us to be able to visualize the internal flow filed in low Prandtl number liquid column.

**Key words:** Marangoni Convection, Low Prandtl Number Fluid, Ultrasonic, Tracer

## 1. Introduction

Marangoni convection is a phenomenon which has long been known but still offers fundamental questions both in science and technology. When a liquid has a nonuniform distribution of temperature or concentration, the distribution of surface tension over free surface also becomes nonuniform, because surface tension generally depends on temperature and concentration. This results in the occurrence of Marangoni convection.

In the present study we investigate temperature-gradient-driven Marangoni convection, especially of half-zone (*HZ*) liquid column (Fig. 1) where the liquid is sustained by surface tension between two disks. We hold the top disk at higher temperature and the bottom disk at lower, so as to suppress buoyancy driven convection. This system has been actively studied for the following reason from a technical point of view; half-zone configuration simulates half the floating-zone (*FZ*) crystallization method. In *FZ* method oscillating Marangoni convection results in the formation of growth striation, which means the deterioration in quality of the produced crystal. Therefore, the grasp and the control of the convection are strongly required.

In low Prandtl number fluid, few experimental works<sup>[1-8]</sup> performed because of its difficulties which were relatively high temperature, necessity of anti-oxidation, measurement of very small temperature change, and so on. By overcoming those difficulties, we detected the transition behavior from axisymmetry to asymmetry steady flow and to oscillatory flow by the very fine temperature measurement<sup>[6]</sup>. However, the flow field has never been observed directly since almost of low Prandtl number fluid (e.g. molten metals and semiconductors) were opaque. So, visualization techniques using a visible

---

\* Japan Aerospace Exploration Agency

\*\* Chiba Institute of Technology

\*\*\* Advanced Engineering Service Co., Ltd.

light could not be used. Therefore, in order to obtain the internal flow pattern directly, the visualization technique using an ultrasonic wave has been developed. Visualization target is thermocapillary convection of molten tin liquid column.

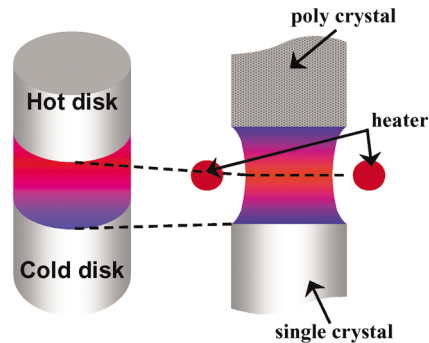


Fig. 1 Half-zone liquid column correspond to Floating-zone crystallization method

## 2. Development of visualization system

### 2.1 Development of transducer

The concept of visualization is quite conventional idea which is particle tracking technique. The three-dimensional positions of particles mixed into the working fluid are detected every moment. Therefore, the flow pattern can be obtained by tracking the tracer positions. Nevertheless, the important issue of the system is how the particle positions can be searched in an opaque liquid. We employed the ultrasonic wave and spherical reflector as a tracer particle. The pulse-like ultrasonic wave was radiated to the working fluid and the echo from the tracers was sensed by eight transducers as shown in Fig. 2. As a result, the particle positions are made clear by a three-dimensional synthetic aperture method. Accordingly, the internal flow pattern can be visualized from dynamic position change of the tracers.

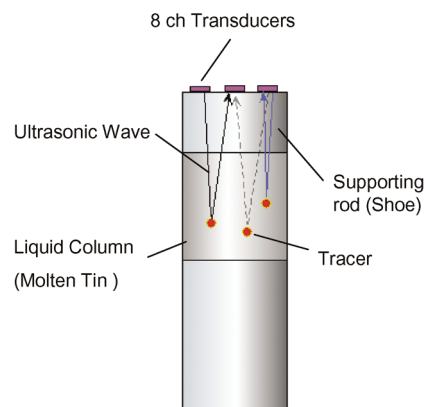


Fig. 2 Concept of Tracer Tracking in Liquid Column Configuration by ultrasonic wave

The transducer/sensor design was determined by utilizing a numerical simulation and some tests. The  $\text{LiNbO}_3$  (LN) single crystal was used as a piezoelectric element which was attached on titanium shoe. Eight array-like piezoelectric elements were attached on titanium shoe which also worked as upper hold rod of liquid column. The interface between titanium shoe and tin liquid column was chromized to avoid the chemical reaction with each other. In this development, the prototype of an integrated sensor was made to verify the sensor performance. The  $\text{LiNbO}_3$  (LN) single crystal as a piezoelectric element was brazed on titanium shoe, which is shown in Fig. 3. Al solder was used to bond the LN element with Ti shoe because this sensor must endure the high temperature around  $450^\circ\text{C}$ . After brazing, LN plate ( $6.6 \times 6.6$  mm) was cut to  $3 \times 3$  matrix element ( $2.1 \times 2.1$  mm) by a saw carefully (Fig. 4). The center of matrix element will not be used

because the electrical wire cannot lead to it. To recover the sensitivity at a high temperature, the heat treatment carried out after molding the electrodes on the LN element.

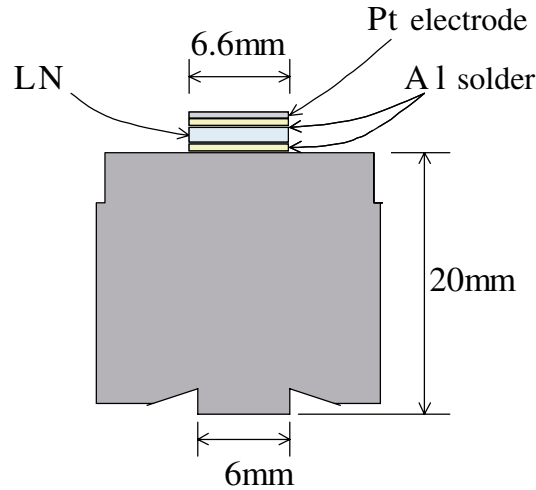


Fig. 3 Schematic of shoe with LN element

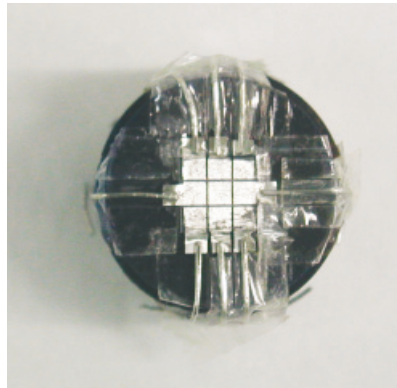


Fig. 4 Sensor after cutting

## 2.2 Sensitivity test

The sensors were checked its sensitivity to compare with both before and after heat treatments. The example of echo signal waveforms is shown in Fig. 5. The peaks from edge face of Ti shoe are clearly observed. Echo peak levels are summarized in Table 1, which are (a) before heat treatment at room temperature, (b) after heat treatment at 500 °C and (c) after heat treatment at room temperature. The average voltage increased more than 10 % by a heat treatment (compare with (a) and (c) in Table 1) and the standard deviation kept almost same. It means that the heat treatment was effective and the sensor was stable with heat up to 500 °C

Table 1 Voltage of Echo signal

Matrix No.	11	12	13	21	23	31	32	33	Ave.	S.D.
Condition (a)	0.234	0.367	0.182	0.328	0.395	0.143	0.412	0.260	0.290	0.101
(b)	0.222	0.357	0.183	0.303	0.398	0.147	0.381	0.244	0.279	0.094
(c)	0.232	0.387	0.182	0.393	0.404	0.217	0.438	0.307	0.320	0.099

Unit : [V]

Ave. : Average

S.D. : Standard Deviation

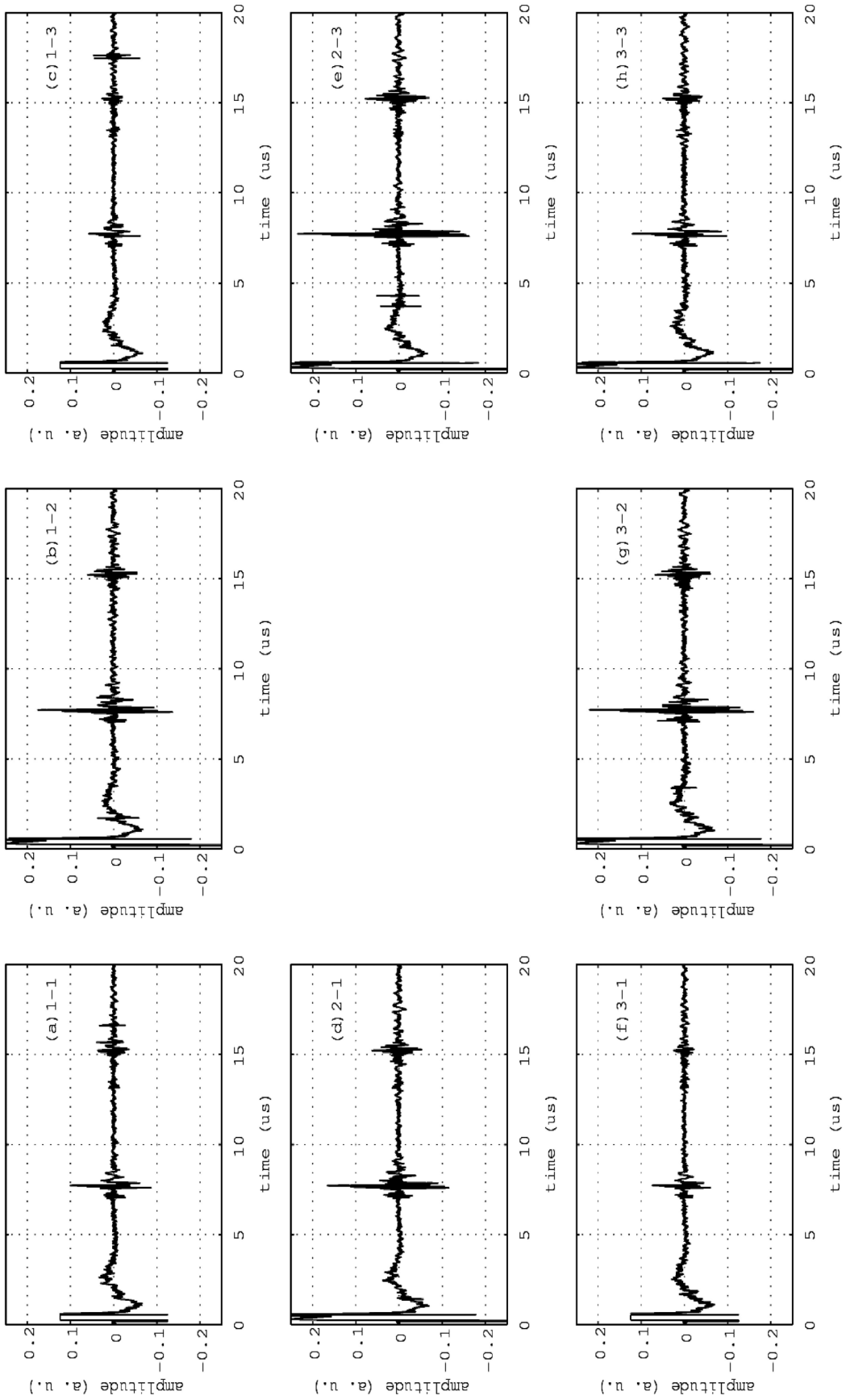


Fig. 5 Waveforms of echo signal form edge face of Ti Shoe after heat treatment at 500 °C

### 2.3 Development for 3D-UV Measuring Unit

Ongoing design of 3D-UV measuring unit is briefly described in this section. In this fiscal year, an oscillator/transmitter was made by determining the specification based on previous conceptual investigations.

At first, we discussed the optimal specification of oscillator. The echo from Ti shoe edge was measured by using a breadboard model sensor that consisted of 2 x 2 sensor element. The frequency band was changed to compare a waveform and S/N ratio as follows:

- (a) 7 to 25 MHz wide-band
- (b) 10 MHz narrow-band (Q=6)
- (c) 10 MHz narrow-band (Q=3)
- (d) 2.5 to 20 MHz wide-band
- (e) 6 to 14 MHz wide-band

The waveform is shown in Fig. 6. The amplitude of echo from shoe edge and S/N ratio is shown in Table 2. S/N ratio was calculated from peak of S1 divided by noise floor between S1 and S2. In the case of case (e) (6 to 14 MHz wide-band), the echo level of S1 became two times higher than other cases, and the character of waveform was improved because the effect of a low frequency component by a pulsive transmitted signal was disappeared.

As a result, the way to improve the character of waveform although it is difficult to reduce the noise floor in the shoe. Therefore, we selected the frequency band of case (e).

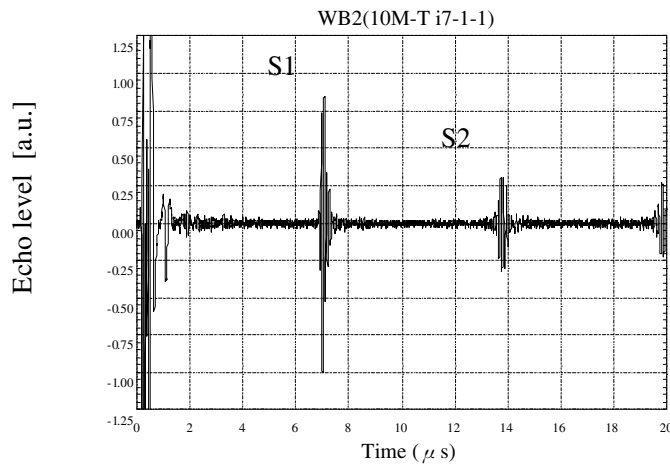


Fig. 6 Waveform in the case of 6 to 14 MHz wide-band

Table 2 Comparison of amplitude of S1 signal and S/N ratio

Frequency band	Amplitude of S1	S/N ratio	mark
(a)	47.3 mVp-p	36.3	Good
(b)	15.1 mVp-p	32.1	Not good
(c)	30.6 mVp-p	34.4	Not good
(d)	43.9 mVp-p	35.7	Good
(e)	81.6 mVp-p	36.5	Very good

For obtaining strong echo signal from a tracer particle, the particles are required to have high reflectance of ultrasonic beam. Since the target value of the reflectance is up to 95 (%), acoustic impedance of a tracer particle should be less than  $0.4 \times 10^6$  (kg/m<sup>2</sup>/s). Considering this acoustic impedance, it is only attainable to make a “balloon like structured trace particle” because acoustic velocity is extremely high.

The employed tracer particles are very small. Therefore, the reflective echo signal would be a very low level. Moreover, the transducers were attached on the shoe in order to protect an *LN* element to the molten tin. While the echo measured with a shoe attenuates, the sound noise by the inside reflection of a shoe was added. For realization of this system, it becomes very important to acquire the echo signal from the tracer by sufficient the signal to noise (*SN*) ratio.

The speed of the ultrasonic wave is very high compared with the speed of the moving tracer. Consequently, the noise which originates in the shoe by the subtraction processing technique was removable. And the *SN* ratio could be improved by the addition processing by repetition measurement, and the *SN* ratio improved about 3 times by calculation supposing actual measurement. Digital data acquisition after the 8ch analog-digital converted. Maximal length interval of sound propagation is 15 ( $\mu$ s) in molten tin liquid column. Run over time on measurement is 150 ( $\mu$ s) in consideration of reverberant sound. Imaging of aperture synthesis is 8 times transmission and 8 times reception on *I* flame. As well averaging procedure is *FPGA* (*Field Programmable Gate Array*) on *A/D* converted hereby speeding up of processing time. This ultrasonic wave echo data was aperture synthesis photographic processing after the delta calculation. Aperture synthesis photographic processing is cut across the liquid column 8 (mm)  $\times$  8 (mm)  $\times$  6 (mm) field about 32  $\times$  32  $\times$  384 mesh size compliant.

### 3. DEVELOPMENT OF TRACER PARTICLE FOR 3D-UV

#### 3.1 Investigation of required conditions as a tracer particle

The base material of a tracer is Shirasu-balloon (*SB*). With regard to the shape as a tracer particle, high sphericity is required. The moderate wettability and low reactivity strongly requires a thin metal coating layer on the *SB* particle too. Therefore, multi-layer structure, which diameter is from 100 to 500 ( $\mu$ m), was adopted as shown in Fig. 7.

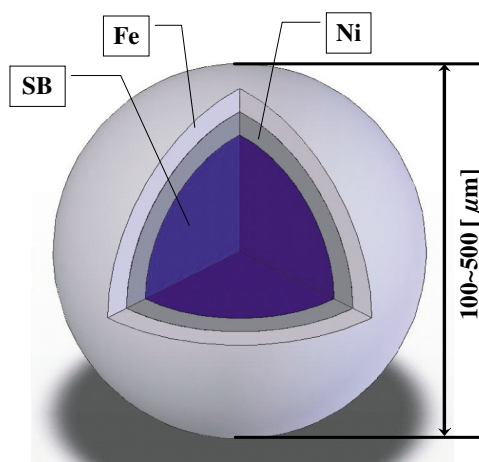


Fig. 7 Schematic diagram of multi-layer Structure Tracer

Table 3 shows the qualitative evaluation of balloons and several porous materials. Selection of *SB*, which is an expanded volcanic particle, as the base material for the tracer particle is reasonable because the *SB* shows high thermal stability and is available size with our target diameter.

The *SB* particles should have following characteristics as tracer particles with surrounding molten tin. With regard to the shape as a tracer particle, high sphericity is also required. The high wettability and low reactivity strongly requires a thin metal coating layer on the *SB* particle. The inner layer plays a role of keeping high sphericity. The *SB* particle is a kind of expanded particles so that its feature was not sphere, and the surface was also rough. Coating the nickel (*Ni*) layer will improve sphericity of the *SB* particle with smooth surface. The outer layer works as a reaction layer with surrounding fluid. The iron (*Fe*) layer reacts with molten tin in moderation, and keeps wettability with surround on surface. The thickness of the layer plays a role of adjusting a density of the *SB* particle with molten tin.

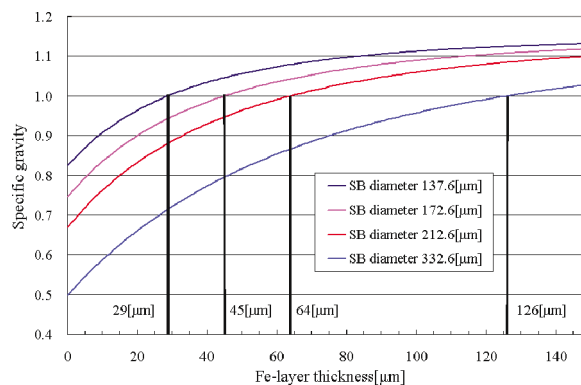
**Table 3** Evaluation of balloons and porous materials

	Sphericity	Available size [ $\mu\text{m}$ ]	Capability to maintain its void in melt	Heat resistance at 773K	Total evaluation
porous $\text{SiO}_2$	○	1-150	×	×	×
porous glass	○	100-500	○	?	×
Shirasu-balloon	△	10-1000	○	○	○
pearlite	×	>150	○	×	×
glass balloon	○	10-100	△	○	△
$\text{Al}_2\text{O}_3$ bubble	×	?	?	○	×
$\text{TiO}_2$ balloon	○	30-50	×	?	×

### 3.2 Consideration Point

Since density of the tracer particle has to be close to that of surrounding fluid, molten tin (approx.  $6.7 \times 10^3$  ( $\text{kg/m}^3$ ) at 673 (K)) for a ground-based experiments, thickness of *Fe* layer should be estimated precisely. The thickness of *Ni* layer is fixed to 40 ( $\mu\text{m}$ ) from the view point of manufacturing technique. The *SB* particle covered with 40 ( $\mu\text{m}$ ) *Ni* layer (*Ni/SB*) is lighter than the molten tin, so that the heavier metal should be plated on the surface so as to adjust the density of the tracer particles with surrounding molten tin. Figure 8 shows the relationship between specific gravity ( $\rho_{\text{tracer}} / \rho_{\text{surround}}$ ) and *Fe* layer thickness. When the *Ni/SB* particle is small (*i.e.* 100-150 ( $\mu\text{m}$ ) in diameter), the thickness of *Fe* plating layer is enough to be only 30-40 ( $\mu\text{m}$ ). However, the large one requires over 100 ( $\mu\text{m}$ ) thickness of *Fe* plating layer. It of course occurs technical issues.

In general, thickness of a film that can be grown by sputtering is only a few microns. Therefore, surface modification of the *SB* particle should be carried out by not sputtering but plating of *Fe*. Since the *SB* shows excellent electric insulation and electroless *Fe* plating is impossible, the plating should be conducted as following processes:

**Fig. 8** Relationship between specific gravity and *Fe* layer thickness for various diameters of the *SB* particles

1<sup>st</sup> stage: Electroless *Ni* plating



2<sup>nd</sup> stage: Electrolysis *Fe* plating



At the viewpoint of traceability of the particles, the maximum diameter of tracer particle must be less than 670 ( $\mu\text{m}$ ) in the case that the molten tin was test fluid. On the other hand, the *3D-UV* system requires that the particle diameter is over 300 ( $\mu\text{m}$ ) in order to detect the signal echo from the particle. Finally, by simple estimation, the overall features of the tracer particle (approx. 300-600 ( $\mu\text{m}$ ) in diameter) will be as follows: diameter of the *SB* is 150-300 ( $\mu\text{m}$ ) and thickness of plating layer of *Ni* and *Fe* are 40 ( $\mu\text{m}$ ) and 35-110 ( $\mu\text{m}$ ), respectively.

Finally, the tracer particles which satisfied above requirements could be manufactured as shown in Fig. 9.

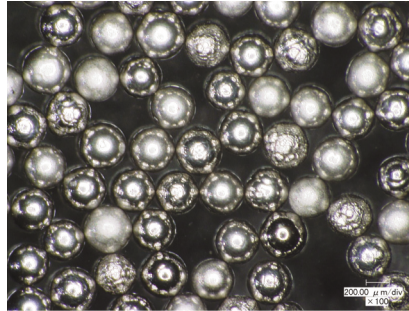


Fig. 9 Photograph of tracer particle of about 300  $\mu\text{m}$  in diameter

## 4. Results of feasibility test

### 4.1 Detectability test

The tracer particle mentioned above was found in a Tin bulk to check the detectability of particle. The position of particle was measured by C-scan probe. Figure 10 shows the result of position measurement of both  $\phi$  1 mm and  $\phi$  0.1 mm particle. This image was drawn from the strength of echo obtained by scanning the ultrasonic beam on the Tin bulk. It can be verified that Fe and Ni plated Shirasu-balloons (Fe-Ni/SB) even in  $\phi$  0.1 mm reflected the ultrasonic. The depth of  $\phi$  1 mm particle was 5 mm from the top and that of  $\phi$  0.1 mm particle was 6 mm. We will use the Tin bulk with a particle to check the sensitivity of matrix sensors.

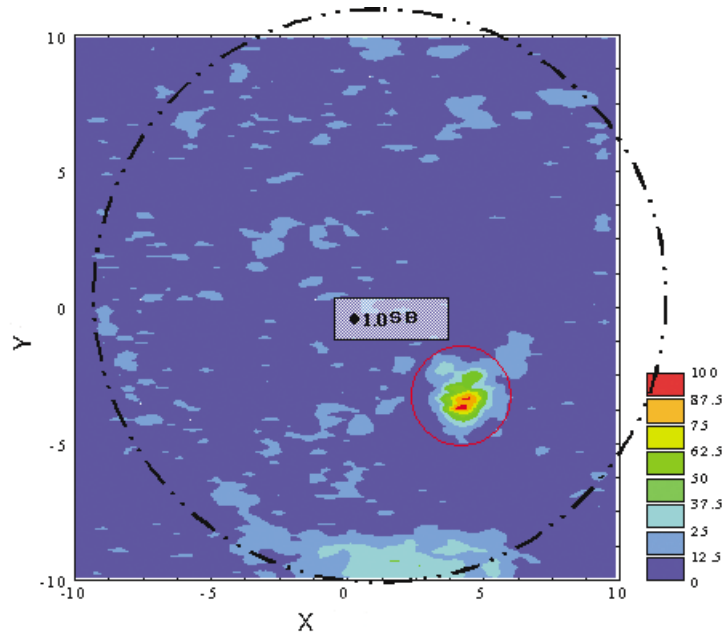
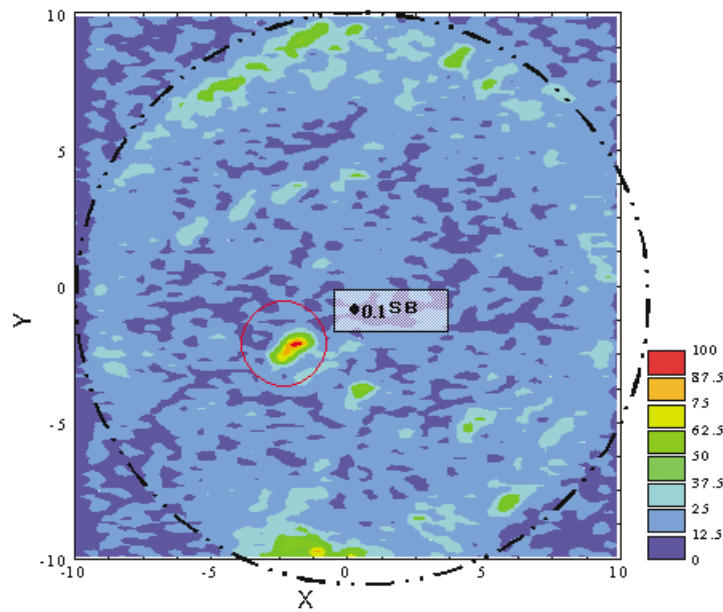
(a)  $\phi$  1 mm particle(b)  $\phi$  0.1 mm particle

Fig. 10 Image of echo signal intensity by C-scan probe

## 4.2 Feasibility test

At first, the feasibility test was performed. A  $\phi$  0.3 (mm) wire was inserted in a liquid bridge of molten tin. Figure 11 shows the visualization result which is voxel expression after the aperture synthesis photographic processing. In Fig. 11, Red region presents wire position which agree well with the actual wire position. Therefore this system could appropriately work even in the high temperature condition around 800 K.

Figure 12 shows the typical results of visualization in the actual configuration, At the upper left cell is X-Y plane viewing angle of molten tin liquid column. At the upper right cell is Y-Z plane viewing angle, and at the lower left cell is X-Z plane viewing angle. We inserted a tracer of 450 ( $\mu$ m) size in the liquid column. Although the small tracer particle, its

position could be revealed. This result demonstrates us to be able to visualize the internal flow field in low Prandtl number liquid column.

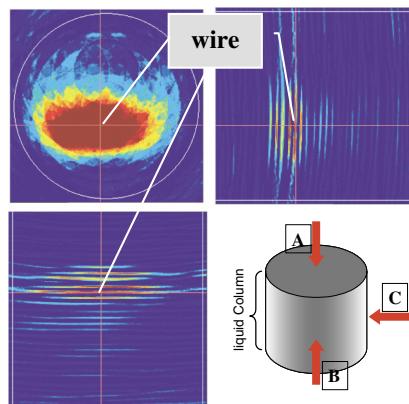


Fig. 11 Feasibility test by thin wire

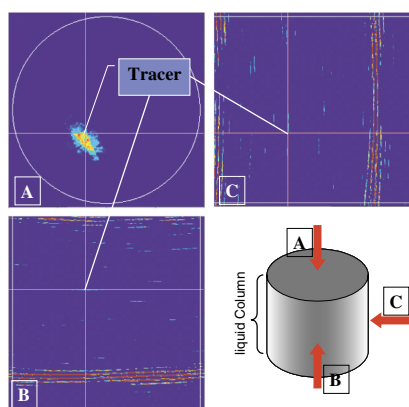


Fig. 12 Feasibility test by tracer particle

## 5. Conclusion

The internal flow visualization system was investigated and manufactured the transducer, signal conditioning system and tracer particles. The *Fe-Ni/SB* tracer particle has been developed. Considering the traceability of the particle, high wettability and low reactivity with surrounding fluid, and high sphericity are required. Therefore, the multi-layer structure, which comprises Fe and Ni layers, was adopted. The plating techniques of both Fe and Ni layers were developed and the heat treatment technique to make the high sphericity particles was also developed. The test particle has already been manufactured and its reflectance of ultrasonic wave has been evaluated. We have performed the feasibility tests for developed system in the actual configuration of Marangoni experiment. In consequence, the visualization of tracer position could be detected.

## References

- [1] Cheng, M. and Kou, S., "Detecting Temperature Oscillation in a Silicon Liquid Bridge", *J. Crystal Growth*, Vol. 218, No. 1, 2000, pp. 132-135.
- [2] Yang, Y. K. and Kou, S., "Temperature Oscillation in a Tin Liquid Bridge and Critical Marangoni Number Dependency on Prandtl Number", *J. Crystal Growth*, Vol. 222, No. 1, 2001, pp. 135-143.

- [3] Matsumoto, S., Hayashida, H., Yoda, S., Komiya, A., Natsui, H., and Imaishi, N., “Transition Phenomena on Marangoni Convection in Low Pr Number Liquid Bridge”, *Thermal Sci. Eng.*, Vol. 12, No. 4, 2004, pp. 21-22
- [4] R. Imai, K. Takagi, M. Ohtaka, F. Ohtsubo, H. Natsui, and S. Yoda, in: *Marangoni Convection Modeling Research Annual Report (NASDA-TMR-990007E)*, National Space Development Agency of Japan (1999) 71.
- [5] K. Takagi, M. Ohtaka, H. Natsui, T. Arai, and S. Yoda, in: *Marangoni Convection Modeling Research Annual Report (NASDA-TMR-000006E)*, National Space Development Agency of Japan (2000) 115.
- [6] NASDA Technical memorandum, *Annual Report of Marangoni Convection Modeling Research*, NASDA-TMR-030004E, (2003) 157.
- [7] K. Takagi, M. Ohtaka, H. Natsui, T. Arai, S. Yoda, Z. Yuan, K. Mukai, S. Yasuhiro, and N. Imaishi, *J. Crystal Growth*, 233 (2001) 399
- [8] M. Ohtaka, K. Takagi, H. Natsui, T. Arai, and S. Yoda, in: *Proc. 2<sup>nd</sup> Pan-Pacific Basin Workshop on Microgravity Sciences*, Pasadena (2001) IF-1159.



## JAXA Research and Development Memorandum JAXA-RM-06-015E

---

Date of Issue : March 30, 2007

Edited and Published by : Japan Aerospace Exploration Agency

7-44-1 Jindaiji-higashimachi, Chofu-shi, Tokyo 182-8522, Japan

URL: <http://www.jaxa.jp/>

Printed by : FUJIPLANS Co., Ltd.

---

Inquires about copyright and reproduction should be addressed to the Aerospace Information Archive Center, Information Systems Department JAXA.

2-1-1 Sengen, Tsukuba-shi, Ibaraki 305-8505, Japan

phone: +81-29-868-5000 fax: +81-29-868-2956

---

Copyright © 2007 by JAXA

All rights reserved. No part of this publication may be reproduced, stored in retrieval system or transmitted, in any form or by any means, electronic, mechanical, photocopying, recording, or otherwise, without permission in writing from the publisher.

